

Predictions of complete fusion cross sections of $^{6,7}\text{Li}$, ^9Be , and ^{10}B with Bayesian neural network method*

Kaixuan Cheng,^{1,†} Rongxing He,¹ Chunyuan Qiao,¹ and Chunwang Ma^{1,2,‡}

¹*School of Physics, Centre for Theoretical Physics, Henan Normal University, Xinxiang 453007, China*

²*Institute of Nuclear Science and Technology, Henan Academy of Sciences, Zhengzhou, 450015, China*

A machine learning approach utilizing the Bayesian neural networks has been developed to predict the complete fusion cross sections of weakly bound nuclei. This method was trained and validated using 475 experimental data points from 39 reaction systems all induced by $^{6,7}\text{Li}$, ^9Be and ^{10}B . The constructed Bayesian neural network demonstrated a high degree of accuracy in evaluating the complete fusion cross sections. By comparing the predicted cross sections with those obtained from the single barrier penetration model, the suppression effect of $^{6,7}\text{Li}$ and ^9Be with stable nucleus was made a systematic analysis. In the cases of ^6Li and ^7Li , a less suppression was predicted at the relatively light mass targets than that found in heavy mass targets and a notably distinct dependence relationship was identified, suggesting that the predominant breakup mechanisms might change in different mass target regions. In addition, the minimum suppression factors are predicted to occur near the target nuclei with neutron closed shell.

Keywords: fusion reaction, weakly bound nuclei, machine learning, Bayesian neural network

I. INTRODUCTION

The advancements in beam quality and detection technology in the latest generation of radiation nuclear beam facilities have brought the study of reaction mechanisms induced by weakly bound nuclei at the Coulomb barrier energy region to the forefront of nuclear physics research [1–5]. In contrast to the fusion processes involving strongly bound nuclei, the mechanisms triggered by weakly bound nuclei are more complex due to their lower binding energies. This complexity is mainly exemplified by the extended nuclear matter distribution and the breakup effect. The former, a static effect, results in a reduction of the average fusion barrier height, consequently enhancing the fusion cross sections. While the dynamic breakup of the projectile can diminish the flux of direct fusion reactions and lead to three distinct processes: (1) sequential complete fusion (SCF), where all fragments resulting from the breakup fuse with the target; (2) incomplete fusion (ICF), where only part of the breakup fragments is absorbed by the target; and (3) no capture breakup (NCBU), where none of the breakup fragments are captured by target. The reaction process in which the whole projectile without breakup is captured by target is termed direct complete fusion (DCF). However, from the experimental perspective, it is challenging to differentiate between the fusion yields of SCF and DCF. As a result, only the complete fusion (CF) cross sections including both DCF and SCF cross sections can be measured.

Numerous experimental and theoretical studies have been performed on fusion reactions involving weakly bound nuclei over the last few decades [6–18]. The main issue in these

studies is to investigate the influence of the breakup on fusion reactions near the Coulomb barrier [19–24]. One of the most widely adopted approaches is to compare the date with the predictions from a single barrier penetration model (BMP) [25, 26] or a coupled channel model without the breakup channels [27, 28]. It has been demonstrated that the CF cross sections are suppressed at energies near and above the Coulomb barrier. So far, the dependence of the suppression effect on the breakup threshold energy of the projectile has been revealed, and an empirical relationship between the suppression factors and the threshold energies is provided in ref. [24]. However, the suppression phenomena with various target nuclei remain incomprehensible [23, 29] and no systematic behavior of the CF suppression factors is observed at the relatively heavy mass target region [1]. For light and medium mass targets, the behavior of the suppression factor is not fully established due to the experimental difficulty in distinguishing residues from ICF and CF. Therefore, we have extended the machine learning method to the fusion reactions induced by weakly bound projectiles and analyzed the systematic behavior of suppression factors across various mass target regions.

Bayesian neural networks (BNNs), as one of the commonly used machine learning methods, have been applied to various issues in nuclear physics, such as predicting atomic nuclear mass [30, 31], nuclear charge radii [32], nuclear β -decay half-life [33], nuclear fission yields [34, 35], spallation reactions [36, 37], and fragmentation reactions [38, 39]. In this paper, based on the 475 experimental data points from 39 reaction systems all induced by $^{6,7}\text{Li}$, ^9Be and ^{10}B , a Bayesian neural network was constructed to evaluate the CF cross sections of weakly bound nuclei. A systematic analysis of the suppression effect at energies above Coulomb barrier has also been conducted. The paper is organized as follows. In Sec. II, the main characteristics of the BNN method are briefly described. The prediction results are discussed in Sec. III. Sec. IV presents a summary.

* Supported by the National Natural Science Foundation of China (Grants No. 12105080 and No. 12375123), the China Postdoctoral Science Foundation (Grants No. 2023M731015), and the Natural Science Foundation of Henan Province (No. 242300422048).

† chengkaixuan@htu.edu.cn

‡ machunwang@126.com

II. MODEL DESCRIPTIONS

As a prominent machine learning technology, Bayesian neural networks are highly effective in constructing novel models based on the existing date. Comprising a specific number of input units, hidden units of several layers, and output units, BNNs are capable of delivering high-quality predictions. Here, a simple description of the BNN methodology is given. More detailed information can be found in refs. [36, 38] and cited therein.

The Bayesian learning sets the prior distribution $p(\omega)$ of the model through the network parameter ω before observing any data, and updates the prior distribution to the posterior distribution $p(\omega|D)$ by observing the experimental data $D(x_i^n, y_j^n)$,

$$p(\omega|D) = \frac{p(D|\omega)p(\omega)}{p(D)} \propto p(D|\omega)p(\omega), \quad (1)$$

where the prior distribution is a Gaussian distribution with zero mean and derived from the initial knowledge of the model. In the observed data $D(x_i^n, y_j^n)$, the outputs y_j^n corresponds to each inputs x_i^n where n, i, j are the number of date, inputs and outputs, respectively. The normalization function, $p(D)$, which ensures the posterior distribution in the effective probability density, is obtained through the model assumptions with a prior integral,

$$p(D) = \int p(D|\omega)p(\omega)d\omega. \quad (2)$$

The likelihood function $p(D|\omega)$ is based on the Gaussian distribution of the objective function χ^2 , which fits the data by least squares,

$$p(D|\omega) = \exp(-\chi^2/2), \quad (3)$$

$$\chi^2 = \sum_{i=1}^N \left[\frac{y_j^n - f_k^n(x_i^n; \omega)}{\Delta y_j^n} \right]^2. \quad (4)$$

Here, Δy_j^n is the Gaussian noise corresponding to the n th observation. The feed-forward neural network is used for the BNN, which structure typically includes a set of input variables, several hidden layers, and one or more output variables. A typical network function that connects outputs y_j^n to inputs x_i^n through one hidden layer is shown as follows,

$$f_k^n(x_i^n; \omega) = a_k + \sum_{j=1}^N b_{jk} \tanh(c_j + \sum_{i=1}^I d_{ij} x_i^n), \quad (5)$$

where N and I are the numbers of hidden units and inputs. (d_{ij}, c_j) and (b_{jk}, a_k) are the weights and biases of the hidden and output layers, respectively. The hidden unit values are obtained by weighted summation of the input values acting on a hyperbolic tangent activation function (tanh), and the outputs $f_k^n(x_i^n; \omega)$ are obtained by weighted summation of the hidden unit values plus biases. The predicted distribution

of output y_j^{n+1} corresponding to the new input x_i^{n+1} can be obtained from the posterior distribution,

$$p(y_j^{n+1}|x_i^{n+1}, D) = \int p(y_j^{n+1}|x_i^{n+1}, \omega)p(\omega|D)d\omega. \quad (6)$$

In the process of calculating output data of the model, Markov chain Monte Carlo method was used to solve the high-dimensional integral,

$$\langle y_j^{n+1} \rangle = \frac{1}{K} \sum_{k=1}^K \int f_k^n(x_i^{n+1}; \omega_k), \quad (7)$$

where K is the number of iteration samples. The uncertainty of predictions is obtained by $\Delta y_j = \sqrt{\langle y_j^2 \rangle - \langle y_j \rangle^2}$ because the model parameters are described with a probability distribution.

In this paper, the dataset comprises the measured CF cross sections in 39 reactions all induced by $^{6,7}\text{Li}$, ^9Be and ^{10}B with 475 data points as detailed in Table 1. Within this dataset, the incident energy of the reactions ranges from $0.67V_b$ to $2.06V_b$, where V_b is the Coulomb barrier energies obtained from Akyüz-Winther nuclear potential and point-sphere Coulomb potential. The mass and charge of the target nuclei fall within the ranges of $64 \leq A_t \leq 209$ and $28 \leq Z_t \leq 83$, respectively. For model development, 80% of the data was randomly selected to form the training set, facilitating the neural networks learning and parameter optimization. The remaining 20% serves as the test set for evaluating the prediction capabilities of the network. The input layer contains five parameters: $\{Z_p, A_p, Z_t, A_t, E_{cm}\}$. Here, Z_p and A_p represent the proton and mass numbers of the projectiles, while Z_t and A_t correspond to those of the targets. The parameter E_{cm} denotes the center-of-mass energy in MeV. The output parameter is the CF cross section, σ_{exp} . Extensive efforts have been made to construct the hidden units, exploring both single-layer and double-layer configurations. The double-layer with 16 + 16 neural units was ultimately verified as the most effective.

III. RESULTS AND DISCUSSIONS

In order to verify the evaluation capacity of BNN model, we perform a comparison between the predicted CF cross sections and the experimental data in Fig. 1. Taking the $^6\text{Li} + ^{159}\text{Tb}$, $^7\text{Li} + ^{209}\text{Bi}$, $^9\text{Be} + ^{89}\text{Y}$, and $^{10}\text{B} + ^{159}\text{Tb}$ systems from the dataset as examples, the predicted results are in good agreement with the experimental CF cross sections, both at sub-barrier energies (Fig. 1(a)) and above barrier energies (Fig. 1(b)). Furthermore, for reaction system $^8\text{Li} + ^{208}\text{Pb}$ [67], which is not included in the dataset, the BNN model also gives the consistent results with the experiment data.

To further investigate the effects of the breakup channel on the fusion of weakly bound systems, a systematic analysis of the suppression factors of CF cross sections at above barrier energies is presented below. The suppression factors are calculated by comparing the CF cross sections obtained from the BNN model or the experimental data with those calculated by

Table 1. The 39 fusion systems induced by weakly bound projectile nuclei ${}^6,7\text{Li}$, ${}^9\text{Be}$ and ${}^{10}\text{B}$. The symbols E_{cm} and V_b are the center-of-mass energy and Coulomb barrier energy, respectively. N_{exp} gives the numbers of experimental CF cross section. F_{BNN} and F_{exp} denote the suppression factors calculated by Eq. (8). The last column is the corresponding reference where the measured cross sections are taken from.

Reaction	$E_{c.m.}/V_B$	N_{exp}	F_{BNN}	F_{exp}	Ref.	Reaction	$E_{c.m.}/V_B$	N_{exp}	F_{BNN}	F_{exp}	Ref.
${}^6\text{Li}+{}^{64}\text{Ni}$	0.85-2.06	15	0.87	0.88	[40]	${}^7\text{Li}+{}^{159}\text{Tb}$	1.07-1.66	5	0.71	0.73	[55]
${}^6\text{Li}+{}^{90}\text{Zr}$	0.82-1.65	8	0.67	0.7	[27]	${}^7\text{Li}+{}^{165}\text{Ho}$	0.86-1.69	10	0.79	0.74	[25]
${}^6\text{Li}+{}^{94}\text{Zr}$	0.89-1.68	5	0.52	0.49	[18]	${}^7\text{Li}+{}^{197}\text{Au}$	0.81-1.50	8	0.84	0.86	[49]
${}^6\text{Li}+{}^{96}\text{Zr}$	0.90-1.58	7	0.77	0.77	[41]	${}^7\text{Li}+{}^{198}\text{Pt}$	0.79-1.52	6	0.72	0.77	[56]
${}^6\text{Li}+{}^{120}\text{Sn}$	0.74-1.32	13	0.78	0.81	[42, 43]	${}^7\text{Li}+{}^{205}\text{Tl}$	0.82-1.31	10	0.77	0.74	[57]
${}^6\text{Li}+{}^{124}\text{Sn}$	0.83-1.70	15	0.72	0.66	[44]	${}^7\text{Li}+{}^{209}\text{Bi}$	0.83-1.67	21	0.75	0.77	[51]
${}^6\text{Li}+{}^{144}\text{Sm}$	0.79-1.58	11	0.55	0.54	[45]	${}^9\text{Be}+{}^{89}\text{Y}$	0.83-1.39	15	0.78	0.75	[58]
${}^6\text{Li}+{}^{152}\text{Sm}$	0.80-1.60	20	0.63	0.62	[46]	${}^9\text{Be}+{}^{93}\text{Nb}$	0.85-1.45	7	0.85	0.90	[59]
${}^6\text{Li}+{}^{154}\text{Sm}$	1.04-1.45	6	0.64	0.71	[47]	${}^9\text{Be}+{}^{124}\text{Sn}$	0.90-1.33	13	0.73	0.75	[60]
${}^6\text{Li}+{}^{159}\text{Tb}$	0.87-1.50	13	0.65	0.66	[48]	${}^9\text{Be}+{}^{144}\text{Sm}$	0.89-1.31	10	0.92	0.94	[61]
${}^6\text{Li}+{}^{197}\text{Au}$	0.84-1.35	16	0.61	0.60	[49]	${}^9\text{Be}+{}^{169}\text{Tm}$	0.93-1.33	12	0.78	0.80	[62]
${}^6\text{Li}+{}^{198}\text{Pt}$	0.67-1.14	10	0.75	0.75	[9]	${}^9\text{Be}+{}^{181}\text{Ta}$	0.94-1.34	13	0.66	0.68	[63]
${}^6\text{Li}+{}^{208}\text{Pb}$	0.92-1.28	20	0.67	0.69	[50]	${}^9\text{Be}+{}^{186}\text{W}$	1.08-1.40	4	0.59	0.57	[64]
${}^6\text{Li}+{}^{209}\text{Bi}$	0.83-1.53	14	0.65	0.68	[51]	${}^9\text{Be}+{}^{187}\text{Re}$	0.93-1.28	12	0.75	0.76	[62]
${}^7\text{Li}+{}^{64}\text{Ni}$	0.87-2.06	16	0.90	0.90	[52]	${}^9\text{Be}+{}^{197}\text{Au}$	0.83-1.17	12	0.78	0.70	[65]
${}^7\text{Li}+{}^{93}\text{Nb}$	1.29-1.63	4	0.75	0.75	[53]	${}^9\text{Be}+{}^{208}\text{Pb}$	0.88-1.24	16	0.78	0.79	[51]
${}^7\text{Li}+{}^{119}\text{Sn}$	0.72-1.30	15	0.93	0.94	[42, 43]	${}^9\text{Be}+{}^{209}\text{Bi}$	0.88-1.21	19	0.98	0.98	[50]
${}^7\text{Li}+{}^{124}\text{Sn}$	0.79-1.86	23	0.71	0.73	[54]	${}^{10}\text{B}+{}^{159}\text{Tb}$	0.91-1.66	16	0.87	0.87	[55]
${}^7\text{Li}+{}^{144}\text{Sm}$	0.88-1.59	14	0.63	0.63	[28]	${}^{10}\text{B}+{}^{209}\text{Bi}$	1.06-1.44	5	0.88	0.89	[66]
${}^7\text{Li}+{}^{152}\text{Sm}$	0.81-1.61	16	0.66	0.69	[28]						

161 the single barrier potential model, as follows,

$$162 \quad F_{BNN} = \frac{\sigma_{BNN}}{\sigma_{BPM}} \quad \text{or} \quad F_{exp} = \frac{\sigma_{exp}}{\sigma_{BPM}}, \quad (8)$$

163 where σ_{BNN} and σ_{exp} are the predicted and measured cross
164 sections, respectively, and σ_{BPM} denotes the cross sections
165 calculated by single barrier potential model. The calculated
166 suppression factors using the predicted CF cross sections and
167 experimental data are listed in the fourth and fifth columns
168 of Table 1. To a large extent, the predictions of BNN model
169 could represent the experimental suppression factors well. A
170 detailed relationship between the suppression factor and the
171 mass number of target nucleus A_t for ${}^6\text{Li}$ and ${}^7\text{Li}$ is shown
172 in Fig. 2(a), and the corresponding results for ${}^9\text{Be}$ and ${}^{10}\text{B}$
173 shown in Fig. 2(b). Those target nuclei are mainly located in
174 the relatively heavy mass region and no obvious dependence
175 behavior can be found. In Fig. 2(a), it is evident that the sup-
176 pression factor of ${}^7\text{Li}$ is larger than the one of ${}^6\text{Li}$ for the same
177 mass target nuclei, which is attributed to the higher breakup
178 threshold energies of ${}^7\text{Li}$ [24].

179 Next, we extend this BNN model to the various mass re-
180 gions of the target nucleus, including the relatively light and

181 medium mass targets. The CF cross sections of ${}^6,7\text{Li}$ and ${}^9\text{Be}$
182 with the target nuclei along β stability line are predicted. The
183 calculated suppression factors versus the neutron, proton, and
184 mass number of targets are shown in Fig. 3. A surprising
185 conclusion is that there is no suppression effect in the vicin-
186 ity of $A_t = 110$ targets for ${}^6,7\text{Li}$ and ${}^9\text{Be}$, as well as $A_t =$
187 180 targets for ${}^6,7\text{Li}$. This is derived from the overall trend of
188 the available experimental data, and further experimental CF
189 cross sections are necessary to verify this conclusion.

190 In Fig. 3, the solid symbols denote the mean suppression
191 factors derived from the targets with identical neutron (a),
192 proton (b), and mass (c) numbers. The dashed error bars
193 illustrate the corresponding distribution range. Taking lead
194 isotopes as an example, the predicted suppression factors of
195 BNN model for ${}^7\text{Li} + {}^{204,206,207,208}\text{Pb}$ are 0.78, 0.77, 0.76,
196 and 0.75, respectively. The mean suppression factor (0.765),
197 the upper limit of the error bar (0.78), and the lower limit of
198 the error bar (0.75) are located at $Z_t = 82$ in the Fig. 3(b).
199 Consequently, the range of error bars indicates the depen-
200 dence relationship of the suppression effect on the isotones,
201 isotopes, and isobars target nuclei. The small error bars of ${}^6\text{Li}$
202 and ${}^7\text{Li}$ suggest a weak dependence, whereas the suppression

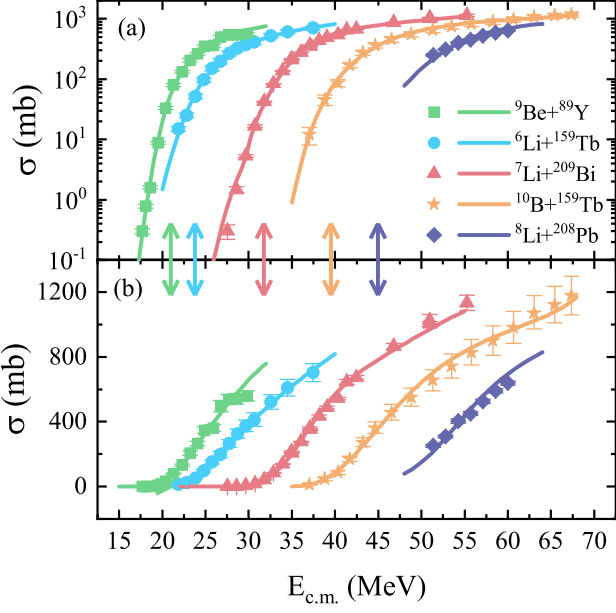


Fig. 1. Comparison of the CF cross sections obtained from the BNN model (solid lines) with the experimental data (solid symbols) for ${}^6\text{Li} + {}^{159}\text{Tb}$, ${}^7\text{Li} + {}^{209}\text{Bi}$, ${}^9\text{Be} + {}^{89}\text{Y}$, ${}^{10}\text{Be} + {}^{159}\text{Tb}$, and ${}^8\text{Li} + {}^{208}\text{Pb}$ systems. The logarithmic scale and linear scale are shown in (a) and (b), respectively. The arrows give the corresponding Coulomb barrier energies. Note that the energies for ${}^7\text{Li} + {}^{209}\text{Bi}$ and ${}^8\text{Li} + {}^{208}\text{Pb}$ are shifted by 1.1 and 1.6, respectively.

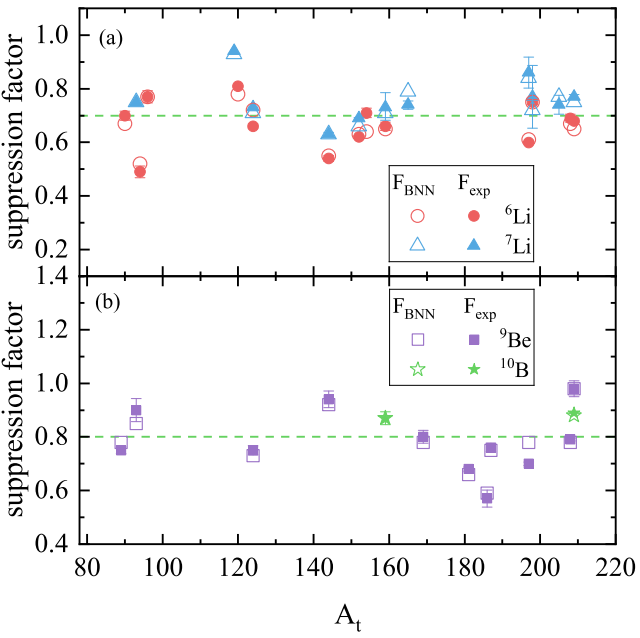


Fig. 2. The suppression factors obtained from the BNN model (open symbols) and experimental data (full symbols) for fusion systems listed in the Tab. 1. The reaction systems induced by ${}^6\text{Li}$, ${}^7\text{Li}$, ${}^9\text{Be}$, and ${}^{10}\text{B}$ are represented by circles, triangles, squares, and stars, respectively. The horizontal dashed lines are the eye guidance reference lines.

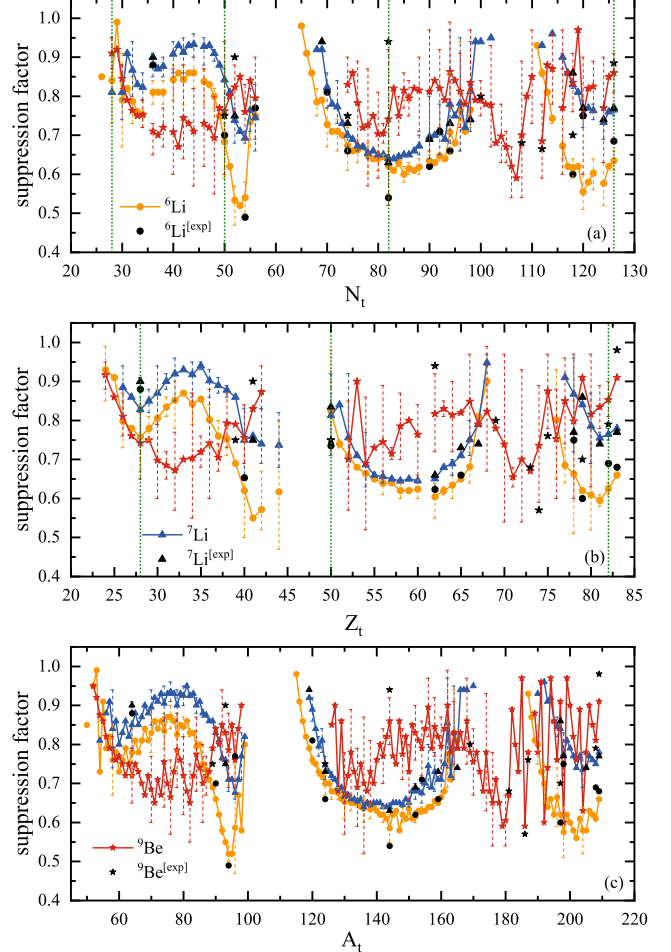


Fig. 3. The relationship between the suppression factors and the neutron (a), proton (b), and mass (c) number of the target nuclei for projectile nuclei ${}^6\text{Li}$ (circle), ${}^7\text{Li}$ (triangle), and ${}^9\text{Be}$ (star). The symbols denote the mean suppression factor and the dashed error bars indicate the distribution range. The magic numbers are located by the vertical dotted lines. The solid lines guide the eye. (See the text for more details.)

203 factors of ${}^9\text{Be}$ exhibit a strong dependence. Due to this sensitivity to the nucleon number of the target nucleus, there is a 204 pronounced fluctuation at various target nuclei for ${}^9\text{Be}$. This, 205 to some extent, brings a difficulty in identifying the systematic 206 trend for ${}^9\text{Be}$.

207 In the cases of ${}^6\text{Li}$ and ${}^7\text{Li}$, the consistent behavior of the 208 mean suppression factor suggests that they possess the similar 209 breakup mechanism, as well as the minimum values of 210 the suppression factor both occurring near the target nuclei 211 with neutron closed shell. Within the relatively light mass 212 target region ($60 \leq A_t \leq 90$), the suppression factors for 213 ${}^6\text{Li}$ and ${}^7\text{Li}$ remain around respectively 0.8 and 0.9, which is 214 significantly less suppression compared to that observed for 215 heavy targets ($120 \leq A_t \leq 160$). Moreover, the systematic 216 behaviors in different mass target regions are markedly 217 distinct. For light mass targets, the suppression factor varies 218 with the target nucleus mass number, initially increasing and 219

220 then decreasing. In contrast, at the heavy mass target re-
 221 gion, the suppression factor initially decreases and then in-
 222 creases. This indicates that there is a competitive process
 223 in the breakup mechanism and the primary breakup channel
 224 may differ across various mass target regions. Due to the lim-
 225 itations of machine learning and complexity of the breakup
 226 processes, it is challenging to provide the specific physical
 227 mechanism here. More experimental and theoretical research
 228 is needed to verify these conclusions and provide more expla-
 229 nations for the underlying breakup mechanism.

230

IV. SUMMARY

231 In this paper, we investigate the complete fusion reactions
 232 of weakly bound nuclei using machine learning methods.
 233 Based on the 475 existing experimental complete fusion data
 234 induced by $^{6,7}\text{Li}$, ^9Be and ^{10}B , a Bayesian neural network is
 235 construct. This model characterizes 5 input parameters (pro-
 236 jectile and target information, colliding energy), double hid-

237 den layers (16+16 neural units), and one output parameter
 238 (CF cross section). The CF cross sections predicted by this
 239 model exhibit an excellent agreement with the experimental
 240 data, demonstrating the model's high-quality predictive ca-
 241 pagilities.

242 The suppression factors, defined as the ratio of the pre-
 243 dicted CF cross sections by BNN model to those calculated by
 244 the single barrier penetration model at above barrier energies,
 245 have been systematically analyzed for weakly bound projec-
 246 tiles $^{6,7}\text{Li}$ and ^9Be with the target nuclei along the β stability
 247 line. The dependence behavior of the suppression effect has
 248 been predicted across various mass target regions, especially
 249 for the relatively light mass targets. For ^9Be , the suppression
 250 factors exhibit marked sensitivity to the target nucleus and no
 251 apparent systematic behavior could be observed in either the
 252 heavy or light mass target regions. In contrast, for ^6Li and
 253 ^7Li , the BNN model predictd a less suppression in relatively
 254 light mass targets compared to that observed for heavy mass
 255 targets. Furthermore, the dependence at the light mass tar-
 256 get region is exactly opposite to that at the heavy mass target
 257 region. These conclusions require further experimental and
 258 theoretical validation, as well as the mechanism explanations.

259 [1] L. F. Canto, P. R. S. Gomes, R. Donangelo et al., 294 <https://doi.org/10.1103/PhysRevLett.103.232702>
 260 Recent developments in fusion and direct reactions 295 [10] S. P. Hu, G. L. Zhang, J. C. Yang et al., Small sup-
 261 with weakly bound nuclei. *Phys. Rept.* **596**, 1 (2015). 296 pression of the complete fusion of the $^6\text{Li} + ^{96}\text{Zr}$ system
 262 <http://doi.org/10.1016/j.physrep.2015.08.001> 297 at near-barrier energies. *Phys. Rev. C* **91**, 044619 (2015).
 263 [2] L. F. Canto, V. Guimaraes, J. Lubian et al., The total reaction 298 <https://doi.org/10.1103/PhysRevC.91.044619>
 264 cross section of heavy-ion reactions induced by stable and un- 299 [11] Y. D. Fang, P. R. S. Gomes, J. Lubian et al., Com-
 265 stable exotic beams: the low-energy regime. *Eur. Phys. J. A* **56**, 300 plete and imcomplete fusion of $^9\text{Be} + ^{169}\text{Tm}$, ^{187}Re at
 266 281 (2020). <https://doi.org/10.1140/epja/s10050-020-00277-8> 301 near barrier energies. *Phys. Rev. C* **91**, 014608 (2015).
 267 [3] K. Hagino, K. Ogata, and A. Moro, Coupled-channels cal- 302 <https://doi.org/10.1103/PhysRevC.91.014608>
 268 culations for nuclear reactions: From exotic nuclei to super- 303 [12] K. J. Cook, E. C. Simpson, L. T. Bezzina et al., Origins of
 269 heavy elements. *Prog. Part. Nucl. Phys.* **125**, 103951 (2022). 304 imcomplete fusion products and the suppression of complete
 270 <https://doi.org/10.1016/j.ppnp.2022.103951> 305 fusion in reactions of ^7Li , *Phys. Rev. Lett.* **122**, 102501 (2019).
 271 [4] Y. L. Ye, X. F. Yang, H. Sakurai et al., Physics 306 <https://doi.org/10.1103/PhysRevLett.122.102501>
 272 of exotic nuclei. *Nat. Rev. Phys.* **7**, 21-37 (2024). 307 [13] L. Jin and A. M. Moro, Puzzle of complete fu-
 273 <https://doi.org/10.1038/s42254-024-00782-5> 308 sion suppression in weakly bound nuclei: a trojan
 274 [5] T. P. Luo, L. Yang, C. J. Lin et al., Reaction dynamics of 309 horse effect? *Phys. Rev. Lett.* **122**, 042503 (2019).
 275 proton-rich nuclei at energies around the Coulomb barrier: the 310 <https://doi.org/10.1103/PhysRevLett.122.042503>
 276 cases of ^7Be , ^8B , and ^{17}F . *Nucl. Sci. Tech.* **35**, 212 (2024). 311 [14] L. Jin and A. M. Moro, Unraveling the reaction
 277 <https://doi.org/10.1007/s41365-024-01586-z> 312 mechanisms leading to partial fusion of weakly
 278 [6] M. Dasgupta, D. J. Hinde, R. D. Butt et al., Fusion 313 bound nuclei. *Phys. Rev. Lett.* **123**, 232501 (2019).
 279 versus breakup: Observation of large fusion suppression 314 <https://doi.org/10.1103/PhysRevLett.123.232501>
 280 for $^9\text{Be} + ^{208}\text{Pb}$. *Phys. Rev. Lett.* **82**, 1395-1398 (1999). 315 [15] K. X. Cheng, J. Pu, Y. T. Wang et al., Non-frozen process of
 281 <https://doi.org/10.1103/PhysRevLett.82.1395> 316 heavy-ion fusion reactions at deep sub-barrier energies. *Nucl.*
 282 [7] D. J. Hinde, M. Dasgupta, B. R. Fulton et al., Fu- 317 *Sci. Tech.* **33**, 132 (2022). <https://doi.org/10.1007/s41365-022-01114-x>
 283 sion Suppression and Sub-Barrier Breakup of Weakly 318 [16] L. Yang, C. J. Lin, H. Yamaguchi et al., Breakup of the proton
 284 Bound Nuclei. *Phys. Rev. Lett.* **89**, 272701(2002). 319 halo nucleus ^8B near barrier energies. *Nat. Commun.* **13**, 7193
 285 <https://doi.org/10.1103/PhysRevLett.89.272701> 320 (2022). <https://doi.org/10.1038/s41467-022-34767-8>
 286 [8] A. D. Torres, D. J. Hinde, J. A. Tostevin et al., Relat- 321 [17] G. L. Zhang, Z. W. Jiao, G. X. Zhang et al., Further
 287 ing Breakup and Incomplete Fusion of Weakly Bound 322 investigation on the fusion of ^6Li with ^{209}Bi target at
 288 Nuclei through a Classical Trajectory Model with 323 near-barrier energies. *Chin. Phys. C* **48**, 074001 (2024).
 289 Stochastic Breakup. *Phys. Rev. Lett.* **98**, 152701 (2007). 324 <https://doi.org/10.1088/1674-1137/ad4264>
 290 <https://doi.org/10.1103/PhysRevLett.98.152701> 325 [18] X. D. Su, G. X. Zhang, S. P. Hu et al., Fusion and one-
 291 [9] A. Shrivastava, A. Navin, A. Lemasson et al., Explor- 326 neutron stripping process for $^6\text{Li} + ^{94}\text{Zr}$ system around
 292 ing Fusion at Extreme Sub-Barrier Energies with Weakly 327 the Coulomb Barrier. *Chin. Phys. C* **48**, 094001 (2024).
 293 Bound Nuclei. *Phys. Rev. Lett.* **103**, 232702 (2009). 328

329 https://doi.org/10.1088/1674-1137/ad50b9
330 [19] K. Hagino, A. Vitturi, C. H. Dasso et al., Role of breakup pro-
331 cesses in fusion enhancement of drip-line nuclei at energies
332 below the Coulomb barrier. *Phys. Rev. C* **61**, 037602 (2000).
333 http://dx.doi.org/10.1103/PhysRevC.61.037602

334 [20] L. R. Gasques, D. J. Hinde, M. Dasgupta et al., Sup-
335 pression of complete fusion due to breakup in the reac-
336 tions $^{10,11}\text{B} + ^{209}\text{Bi}$. *Phys. Rev. C* **79**, 034605 (2009).
337 http://dx.doi.org/10.1103/PhysRevC.79.034605

338 [21] M. Dasgupta, L. R. Gasques, D. H. Luong et al.,
339 Reaction dynamics of weakly bound nuclei at near-
340 barrier energies. *Nucl. Phys. A* **834**, 147c–150c (2010).
341 http://dx.doi.org/10.1016/j.nuclphysa.2009.12.025

342 [22] P. R. S. Gomes, D. R. Otomar, T. Correa et al., Complete fu-
343 sion enhancement and suppression of weakly bound nuclei at
344 near barrier energies. *J. Phys. G: Nucl. Part. Phys.* **39**, 115103
345 (2012). http://dx.doi.org/10.1088/0954-3899/39/11/115103

346 [23] V. V. Sargsyan, G. G. Adamian, N. V. Antonenko et al.,
347 Search for a systematic behavior of the breakup probabili-
348 ty in reactions with weakly bound projectiles at energies
349 around the Coulomb barrier. *Phys. Rev. C* **86**, 054610 (2012).
350 http://dx.doi.org/10.1103/PhysRevC.86.054610

351 [24] B. Wang, W. J. Zhao, P. R. S. Gomes et al., System-
352 atic study of breakup effects on complete fusion at energies
353 above the Coulomb barrier. *Phys. Rev. C* **90**, 034612 (2014).
354 http://dx.doi.org/10.1103/PhysRevC.90.034612

355 [25] V. Tripathi, A. Navin, K. Mahata et al., Angular Momen-
356 tum and Cross Sections for Fusion with Weakly Bound Nu-
357 clei: Breakup, a Coherent Effect. *Phys. Rev. Lett.* **88**, 172701
358 (2002). http://dx.doi.org/10.1103/PhysRevLett.88.172701

359 [26] V. Tripathi, A. Navin, V. Nanal et al., Experimental
360 signatures for distinguishing breakup fusion and trans-
361 fer in $^7\text{Li} + ^{165}\text{Ho}$. *Phys. Rev. C* **72**, 017601 (2005).
362 http://dx.doi.org/10.1103/PhysRevC.72.017601

363 [27] H. Kumawat1, V. Jha1, V. V. Parkar et al., Fusion
364 reaction studies for the $^6\text{Li} + ^{90}\text{Zr}$ system at near-
365 barrier energies. *Phys. Rev. C* **86**, 024607 (2012).
366 http://dx.doi.org/10.1103/PhysRevC.86.024607

367 [28] P. K. Rath1, S. Santra, N. L. Singh et al., Complete fusion in
368 $^7\text{Li} + ^{144,152}\text{Sm}$ reactions. *Phys. Rev. C* **88** 044617 (2013).
369 http://dx.doi.org/10.1103/PhysRevC.88.044617

370 [29] P. R. S. Gomes, R. Linares, J. Lubian et al., Search
371 for systematic behavior of incomplete-fusion probabili-
372 ty and complete-fusion suppression induced by ^9Be
373 on different targets. *Phys. Rev. C* **84**, 014615 (2011).
374 http://dx.doi.org/10.1103/PhysRevC.84.014615

375 [30] Z. M. Niu and H. Z. Liang, Nuclear mass predictions
376 based on Bayesian neural network approach with pair-
377 ing and shell effects. *Phys. Lett. B* **778**, 48 (2018).
378 http://dx.doi.org/10.1016/j.physletb.2018.01.002

379 [31] Z. M. Niu and H. Z. Liang, Nuclear mass predictions
380 with machine learning reaching the accuracy required by
381 r-process studies. *Phys. Rev. C* **106**, L021303 (2022).
382 http://dx.doi.org/10.1103/PhysRevC.106.L021303

383 [32] Y. F. Ma, C. Su, J. Liu et al., Predictions of nuclear charge
384 radii and physical interpretations based on the naive Bayesian
385 probability classifier. *Phys. Rev. C* **101**, 014304 (2020).
386 http://dx.doi.org/10.1103/PhysRevC.101.014304

387 [33] Z. M. Niu, H. Z. Liang, B. H. Sun et al., Predictions of nuclear
388 β -decay half-lives with machine learning and their impact on
389 r-process nucleosynthesis. *Phys. Rev. C* **99**, 064307 (2019).
390 http://dx.doi.org/10.1103/PhysRevC.99.064307

391 [34] C. Y. Qiao, J. C. Pei, Z. A. Wang et al., Bayesian
392 evaluation of charge yields of fission fragments
393 of ^{239}U . *Phys. Rev. C* **103**, 034621 (2021).
394 http://dx.doi.org/10.1103/PhysRevC.103.034621

395 [35] Z. A. Wang, J. C. Pei, Y. Liu et al., Bayesian Evaluation of
396 Incomplete Fission Yields. *Phys. Rev. Lett.* **123**, 122501 (2019).
397 http://dx.doi.org/10.1103/PhysRevLett.123.122501

398 [36] C. W. Ma, D. Peng, H. L. Wei, Isotopic cross-sections in
399 proton induced spallation reactions based on the Bayesian
400 neural network method. *Chin. Phys. C* **44**, 014104 (2020).
401 http://dx.doi.org/10.1088/1674-1137/44/1/014104

402 [37] C. W. Ma, D. Peng, H. L. Wei et al., A Bayesian-Neural-
403 Network Prediction for Fragment Production in Proton In-
404duced Spallation Reaction. *Chin. Phys. C* **44**, 124107 (2020).
405 http://dx.doi.org/10.1088/1674-1137/abb657

406 [38] C. W. Ma, X. B. Wei, X. X. Chen et al., Precise machine learn-
407 ing models for fragment production in projectile fragmentation
408 reactions using Bayesian neural networks. *Chin. Phys. C* **46**,
409 074104 (2022). http://dx.doi.org/10.1088/1674-1137/ac5efb

410 [39] C. W. Ma, X. X. Chen, X. B. Wei et al., Systematic behavior
411 of fragments in Bayesian neural network models for projec-
412 tile fragmentation reactions. *Phys. Rev. C* **108**, 044606 (2023).
413 http://dx.doi.org/10.1103/PhysRevC.108.044606

414 [40] M. M. Shaikh, S. Roy, S. Rajbanshi et al., Investigation of $^6\text{Li} + ^{64}\text{Ni}$ fusion at near-barrier energies. *Phys. Rev. C* **90**, 024615
415 (2014). http://dx.doi.org/10.1103/PhysRevC.90.024615

416 [41] S. P. Hu, G. L. Zhang, J. C. Yang et al., Small sup-
417 pression of the complete fusion of the $^6\text{Li} + ^{96}\text{Zr}$ system
418 at near-barrier energies. *Phys. Rev. C* **91**, 044619 (2015).
419 http://dx.doi.org/10.1103/PhysRevC.91.044619

420 [42] N. Grover, I. Sharma, M. S. Gautam et al., Fusion and de-
421 cay dynamics of $^6\text{Li} + ^{120}\text{Sn}$ and $^7\text{Li} + ^{119}\text{Sn}$ reactions
422 across the Coulomb barrier. *Phys. Rev. C* **108**, 064607 (2023).
423 http://dx.doi.org/10.1103/PhysRevC.108.064607

424 [43] M. Fisichella1, A. C. Shotter, P. Figueral et al., Breakup and
425 n-transfer effects on the fusion reactions $^{6,7}\text{Li} + ^{120,119}\text{Sn}$
426 around the Coulomb barrier. *Phys. Rev. C* **95**, 034617 (2017).
427 http://dx.doi.org/10.1103/PhysRevC.95.034617

428 [44] V. V. Parkar1, S. K. Pandit1, A. Shrivastava et al., Fu-
429 sion reaction studies for the $^6\text{Li} + ^{124}\text{Sn}$ system at
430 near-barrier energies. *Phys. Rev. C* **98**, 014601 (2018).
431 http://dx.doi.org/10.1103/PhysRevC.98.014601

432 [45] P. K. Rath, S. Santra, N. L. Singh et al., Sup-
433 pression of complete fusion in the $^6\text{Li} + ^{144}\text{Sm}$
434 reaction. *Phys. Rev. C* **79**, 051601 (2009).
435 http://dx.doi.org/10.1103/PhysRevC.79.051601

436 [46] P. K. Rath, S. Santra, N. L. Singh et al., Fusion
437 of ^6Li with ^{152}Sm : Role of projectile breakup ver-
438 sus target deformation. *Nucl. Phys. A* **874**, 14 (2012).
439 http://dx.doi.org/10.1016/j.nuclphysa.2011.10.004

440 [47] C. L. Guo, G. L. Zhang, S. P. Hu et al., Coupling ef-
441 fects on the fusion of $^6\text{Li} + ^{154}\text{Sm}$ at energies slightly
442 above the Coulomb barrier. *Phys. Rev. C* **92**, 014615 (2015).
443 http://dx.doi.org/10.1103/PhysRevC.92.014615

444 [48] M. K. Pradhan, A. Mukherjee, P. Basu et al., Fusion of ^6Li with
445 ^{159}Tb at near barrier energies. *Phys. Rev. C* **83**, 064606 (2011).
446 http://dx.doi.org/10.1103/PhysRevC.83.064606

447 [49] C. S. Palshetkar1, S. Thakur, V. Nanal et al., Fusion and quasi-
448 elastic scattering in the $^{6,7}\text{Li} + ^{197}\text{Au}$ systems. *Phys. Rev. C*
449 **89**, 024607 (2014). [Erratum: *Phys. Rev. C* **100**, 039902 (2019)]
450 http://dx.doi.org/10.1103/PhysRevC.89.024607

451 [50] Z. H. Liu, C. Signorini, M. Mazzocco et al., Partial fusion
452 of a weakly bound projectile with heavy target at energies
453 above the Coulomb barrier. *Eur. Phys. J. A* **26**, 73 (2005).
454

455 http://dx.doi.org/10.1140/epja/i2004-10305-4

456 [51] M. Dasgupta¹, P. R. S. Gomes, D. J. Hinde et al., Ef-
457 fect of breakup on the fusion of ^6Li , ^7Li , and ^9Be
458 with heavy nuclei. *Phys. Rev. C* **70**, 024606 (2004).
459 http://dx.doi.org/10.1103/PhysRevC.70.024606

460 [52] M. M. Shaikh, S. Roy, S. Rajbanshi et al., Probing the fusion of
461 ^7Li with ^{64}Ni at near-barrier energies. *Phys. Rev. C* **93**, 044616
462 (2016). http://dx.doi.org/10.1103/PhysRevC.93.044616

463 [53] S. K. Pandit¹, A. Shrivastava, K. Mahata et al., In-
464 vestigation of large α production in reactions involving
465 weakly bound ^7Li . *Phys. Rev. C* **96**, 044616 (2017).
466 http://dx.doi.org/10.1103/PhysRevC.96.044616

467 [54] V. V. Parkar, S. K. Sharma, R. Palit et al., Investigation of com-
468 plete and incomplete fusion in the $^7\text{Li} + ^{124}\text{Sn}$ reaction near
469 Coulomb barrier energies. *Phys. Rev. C* **97**, 014607 (2018).
470 http://dx.doi.org/10.1103/PhysRevC.97.014607

471 [55] A. Mukherjee, S. Roy, M. K. Pradhan et al., In-
472 fluence of projectile alpha- breakup threshold on
473 complete fusion. *Phys. Lett. B* **636**, 91 (2006).
474 http://dx.doi.org/10.1016/j.physletb.2006.03.051

475 [56] A. Shrivastava, A. Navin, A. D. Torres et al., Role
476 of the cluster structure of ^7Li in the dynamics of
477 fragment capture. *Phys. Lett. B* **718**, 931 (2013).
478 http://dx.doi.org/10.1016/j.physletb.2012.11.064

479 [57] V. V. Parkar, M. Prasanna, R. Ruchi et al., Fusion of ^7Li
480 with ^{205}Tl at near-barrier energies. *Phys. Rev. C* **109**, 014610
481 (2024). http://dx.doi.org/10.1103/PhysRevC.109.014610

482 [58] C. S. Palshetkar, S. Santra, A. Chatterjee et al., Fusion of the
483 weakly bound projectile ^9Be with ^{89}Y . *Phys. Rev. C* **82**, 044608
484 (2010). http://dx.doi.org/10.1103/PhysRevC.82.044608

485 [59] H. Sharma, M. Maiti, M. Sagwa et al., Study of ^9Be fusion in
486 ^{93}Nb near the Coulomb barrier. *Eur. Phys. J. A* **60**, 64 (2024).
487 http://dx.doi.org/10.1140/epja/s10050-024-01296-5

488 [60] V. V. Parkar, R. Palit¹, S. K. Sharma et al., Fusion cross
489 sections for the $^9\text{Be} + ^{124}\text{Sn}$ reaction at energies near
490 the Coulomb barrier. *Phys. Rev. C* **82**, 054601 (2010)
491 http://dx.doi.org/10.1103/PhysRevC.82.054601

492 [61] P. R. S. Gomesa, J. Lubiana, B. Paes et al., Near-
493 barrier fusion, breakup and scattering for the ^9Be
494 + ^{144}Sm system. *Nucl. Phys. A* **828**, 233 (2009).
495 http://dx.doi.org/10.1016/j.nuclphysa.2009.07.008

496 [62] Y. D. Fang, P. R. S. Gomes, J. Lubian et al., Com-
497 plete and incomplete fusion of $^9\text{Be} + ^{169}\text{Tm}$, ^{187}Re at
498 near-barrier energies. *Phys. Rev. C* **91**, 014608 (2015).
499 http://dx.doi.org/10.1103/PhysRevC.91.014608

500 [63] N. T. Zhang, Y. D. Fang, P. R. S. Gomes et al.,
501 Complete and incomplete fusion in the $^9\text{Be} +$
502 ^{181}Ta reaction. *Phys. Rev. C* **90**, 024621 (2014).
503 http://dx.doi.org/10.1103/PhysRevC.90.024621

504 [64] Y. D. Fang, P. R. S. Gomes, J. Lubian et al., Fusion and
505 one-neutron stripping reactions in the $^9\text{Be} + ^{186}\text{W}$ system
506 above the Coulomb barrier. *Phys. Rev. C* **87**, 024604 (2013).
507 http://dx.doi.org/10.1103/PhysRevC.87.024604

508 [65] M. Kaushik, G. Gupta, S. Thakur et al., Fusion of
509 the Borromean nucleus ^9Be with a ^{197}Au target at
510 near-barrier energies. *Phys. Rev. C* **101**, 034611 (2020).
511 http://dx.doi.org/10.1103/PhysRevC.101.034611

512 [66] L. R. Gasques, D. J. Hinde, M. Dasgupta et al., Sup-
513 pression of complete fusion due to breakup in the reac-
514 tions $^{10,11}\text{B} + ^{209}\text{Bi}$. *Phys. Rev. C* **79**, 034605 (2009).
515 http://dx.doi.org/10.1103/PhysRevC.79.034605

516 [67] E. F. Aguilera, E. M. Quiroz, P. Rosales et al., Hin-
517 drance of complete fusion in the $^8\text{Li} + ^{208}\text{Pb}$ system at
518 above-barrier energies. *Phys. Rev. C* **80**, 044605 (2009).
519 http://dx.doi.org/10.1103/PhysRevC.80.044605